Journal of Solid State Chemistry 184 (2011) 2490–2497

Contents lists available at ScienceDirect

Journal of Solid State Chemistry

journal homepage: www.elsevier.com/locate/jssc

High-pressure synthesis and crystal structure of the lithium borate HP-LiB_3O_5

Stephanie C. Neumair [a], Stefan Vanicek [a], Reinhard Kaindl [b,1], Daniel M. Többens [b], Klaus Wurst [a], Hubert Huppertz [a,*]

[a] Institut für Allgemeine, Anorganische und Theoretische Chemie, Leopold-Franzens-Universität Innsbruck, Innrain 52a, A-6020 Innsbruck, Austria
[b] Institut für Mineralogie und Petrographie, Leopold-Franzens-Universität Innsbruck, Innrain 52, A-6020 Innsbruck, Austria

ARTICLE INFO

Article history:
Received 13 May 2011
Received in revised form
9 July 2011
Accepted 10 July 2011
Available online 19 July 2011

Keywords:
Lithium borate
Borate
High pressure
Multianvil
Crystal structure

ABSTRACT

The new lithium borate HP-LiB_3O_5 was synthesized under high-pressure/high-temperature conditions of 6 GPa and 1050 °C in a multianvil press with a Walker-type module. The compound crystallizes in the space group *Pnma* (no. 62) with the lattice parameters $a=829.7(2)$, $b=759.6(2)$, and $c=1726.8(4)$ pm ($Z=16$). The high-pressure compound HP-LiB_3O_5 is built up from a three-dimensional network of BO_4 tetrahedra and BO_3 groups, which incorporates Li^+ ions in channels along the *b*-axis. Band assignments of measured IR- and Raman spectra were done via quantum-mechanical calculations. Additionally, the thermal behavior of HP-LiB_3O_5 was investigated.

1. Introduction

Alongside with characterization and synthesis of new borates, several new applications for these compounds were established in the last decades. Among others, the interest in nonlinear optical effects of non-centrosymmetric borates has grown considerably. Since the technical development of β-BaB_2O_4, which proved to be excellent for frequency conversion, many borates have been examined [1].

One example is the ambient pressure phase LiB_3O_5 [2], which is now widely used as a material for nonlinear optical units and integrated optical waveguides in surgery, radar, laser weapons, etc. This lithium borate not only exhibits remarkable nonlinear optical properties [3–5], but also spontaneous polarization and moderate piezoelectric coefficients [6,7], parallel with high laser damage threshold as well as luminescent properties [8,9]. The ambient pressure phase LiB_3O_5 crystallizes in the space group $Pna2_1$ and is built up by a framework of triborate rings, consisting of two BO_3 units and a BO_4 tetrahedron. The Li^+ ions are located in the interspaces of this framework.

Next to LiB_3O_5, various compounds exist in the ternary system Li–B–O, e.g. $Li_2B_4O_7$ [10–13], $LiBO_2$ [14,15], and $Li_3B_7O_{12}$ [16]. The lithium tetraborate $Li_2B_4O_7$ exhibits further useful physical properties such as thermoluminescence and ionic conductivity. In compounds containing lithium, ionic conduction is of particular interest, as recent developments of electric vehicles increase the need for new battery materials with higher energy density and very long lifespans. Moreover, $Li_2B_4O_7$ and $LiBO_2$, or mixture of both is used as borate fusion flux during the sample preparation for inductively coupled plasma atomic emission spectroscopy (ICP-AES), or X-ray fluorescence spectroscopy (XRF).

Investigating borates by high-pressure/high-temperature, we were able to synthesize a high-pressure modification of LiB_3O_5. In contrast to the non-centrosymmetric phase LiB_3O_5, the high-pressure modification HP-LiB_3O_5 is centrosymmetric. In this paper, we describe the synthesis, the crystal structure, and the properties of HP-LiB_3O_5.

2. Experimental section

2.1. Synthesis

The new borate HP-LiB_3O_5 was synthesized under high-pressure/high-temperature conditions in a modified Walker-type module in combination with a 1000 t press (both devices from the company Voggenreiter, Mainleus, Germany). As pressure medium, a

* Corresponding author. Fax: +43 512 5072934.
E-mail address: Hubert.Huppertz@uibk.ac.at (H. Huppertz).
[1] Present address: JOANNEUM RESEARCH Forschungsgesellschaft mbH, MATERIALS - Institut für Oberflächentechnologien und Photonik, Funktionale Oberflächen, Leobner Strasse 94, A-8712 Niklasdorf, Austria.

0022-4596/$ - see front matter © 2011 Elsevier Inc. All rights reserved.
doi:10.1016/j.jssc.2011.07.011

precastable MgO-octahedron (Ceramic Substrates & Components, Isle of Wight, UK) with an edge length of 18 mm was used. Eight tungsten carbide cubes (TSM 10, Ceratizit, Austria) with a truncation edge length of 11 mm compressed the octahedron (18/11-assembly). According to Eq. (1), Li_2O (99.5%, Alfa Aesar, Karlsruhe, Germany) and B_2O_3 (99.9%, Strem Chemicals, Newburyport, USA) were mixed, ground together, and filled into a boron nitride crucible (BNP GmbH, HeBoSint® S10, Germany). Further information on the construction of the assembly is given in Refs. [17–21].

$$Li_2O + 3\ B_2O_3 \xrightarrow[6\,GPa]{1050\,^{\circ}C} 2\ HP\text{-}LiB_3O_5 \quad (1)$$

The assembly was compressed to 6 GPa within 3 h, followed by a heating period of 10 min, in which the sample reached a temperature of 1050 °C. The temperature was held for 10 min, decreased to 400 °C within 40 min and finally quenched to room temperature by switching off the heating. After the decompression (9 h), the recovered MgO octahedron was broken apart in order to isolate the sample for further analytical investigations. Surrounding hexagonal boron nitride from the crucible was carefully separated from the sample, to obtain the air-resistant compound HP-LiB_3O_5 in the form of large colorless crystals.

2.2. Crystal structure analysis

The sample was characterized by X-ray powder diffraction, using a Stoe Stadi P powder diffractometer with transmission geometry and monochromatized Mo$K\alpha_1$ (λ=70.93 pm) radiation. The powder diffraction pattern (Fig. 1) showed reflections of HP-LiB_3O_5 as well as another yet unknown phase (marked with asterisks). The experimental powder pattern fits well with the theoretical powder pattern, simulated from the single crystal data. The reflections of the lithium borate were indexed with the program Treor [22] on the basis of an orthorhombic unit cell. The lattice parameters (Table 1) were calculated from least-squares fits of the powder data. The correct indexing of the pattern of HP-LiB_3O_5 was confirmed by intensity calculations, taking the atomic positions from the single crystal structure refinement [23].

For the single-crystal structure analysis, small irregularly shaped crystals of HP-LiB_3O_5 were isolated by mechanical fragmentation. Measurements of the single-crystal intensity data took place at room temperature by a Nonius Kappa CCD 4-circle diffractometer, using graphite monochromatized Mo$K\alpha$ (λ=71.073 pm) radiation, a Micracol Fiber Optics collimator, and a Nonius FR590 generator. A semiempirical absorption correction based on equivalent and redundant intensities (Scalepack [24]) was applied to the intensity data. All relevant details of the data collections and evaluations are listed in Table 1.

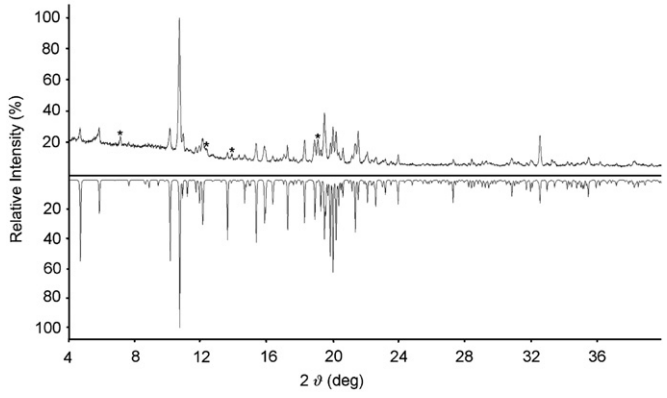

Fig. 1. Experimental powder pattern (top), compared with a theoretical powder pattern of HP-LiB_3O_5 (bottom); the reflections marked with an asterisk arise from a yet unknown phase.

Table 1
Crystal data and structure refinement of HP-LiB_3O_5.

Empirical formula	HP-LiB_3O_5
Molar mass, g mol^{-1}	119.37
Crystal system	orthorhombic
Space group	*Pnma* (no. 62)
Powder diffractometer	Stoe Stadi *P*
Radiation	Mo$K\alpha_1$ (λ=70.93 pm) (Ge(1 1 1)-monochromator)
Powder data	
a, pm	829.9(2)
b, pm	759.9(2)
c, pm	1727.6(3)
V, nm^3	1.0895(3)
Single crystal diffractometer	Enraf-Nonius Kappa CCD
Radiation	Mo$K\alpha$ (λ=71.073 pm) (graphite monochromator)
Single crystal data	
a, pm	829.7(2)
b, pm	759.6(2)
c, pm	1726.8(4)
V, nm^3	1.088(1)
Formula units per cell	Z=16
Calculated density, g cm^{-3}	2.914
Crystal size, mm^3	0.24 × 0.21 × 0.1
Temperature, K	293(2)
Detector distance, mm	36.0
Exposure time, s	60
Absorption coefficient, mm^{-1}	0.271
F(0 0 0), e	928
θ range, deg.	2.4–37.8
Range in *h k l*	−13/+14; ±13; −26/+29
Reflections total/independent	16352/3085
R_{int}	0.0320
Reflections with $I \geq 2\sigma(I)$	2700
R_σ	0.0244
Data/ref. parameters	3085/179
Absorption correction	multi-scan (Scalepack [24])
Final *R*1/*wR*2 [$I \geq 2\sigma(I)$]	0.0300/0.0772
Final *R*1/*wR*2 (all data)	0.0358/0.0808
Goodness-of-fit on F^2	1.038
Largest diff. peak and hole, e Å^{-3}	0.41/−0.32

According to the systematic extinctions, the space groups $Pna2_1$ (No. 33) and *Pnma* (No. 62) were derived. The centrosymmetric space group *Pnma* was found to be correct during the refinement. This was confirmed with the Addsym routine of the program Platon [25]. The structure solution and parameter refinement (full matrix least squares on F^2) were successfully performed using the Shelx-97 software suite [26,27]. All atoms were refined with anisotropic displacement parameters. The final difference Fourier syntheses did not reveal any significant peaks in the refinements. Tables 2–4 show the positional parameters, the anisotropic displacement parameters, and selected interatomic distances. Further details of the crystal structure investigation may be obtained from the Fachinformationszentrum Karlsruhe, D-76344 Eggenstein-Leopoldshafen, Germany (fax: +49 7247 808 666; e-mail: mcrysdata@fiz-karlsruhe.dea, http://www.fizinformationsdienste.de/en/DB/icsd/ depot _anforderung.html) on quoting the deposition number CSD-422922.

3. Results and discussion

3.1. Crystal structure of HP-LiB_3O_5

The new borate HP-LiB_3O_5 was synthesized under high-pressure/high-temperature conditions of 6 GPa and 1050 °C from molar ratios of the pure oxides Li_2O and B_2O_3 (see Section 2).

Figs. 2 and 3 show the crystal structure of HP-LiB_3O_5 with a view along [0 $\bar{1}$ 0] and [$\bar{1}$ 0 0], respectively (single crystal data see Tables 1–4). The structure is built up from segments of corner-sharing BO_4 tetrahedra, which are interconnected to ribbons running along the *a*-axis. The ribbons are condensed to massive sheets in the ab-plane, that are interconnected via trigonal-planar BO_3 units, generating channels along the *b*-axis, in which the Li^+ ions are situated. As shown in Fig. 3, the connecting BO_3 units form pyroborate ($[B_2O_5]^{4-}$) units via corner-sharing. To some extent, the structure resembles the ionic conductor β-alumina, which comprises alternating massive spinell blocks and conduction planes containing the mobile cations [28].

From the 13 crystallographically independent oxygen ions, O4, O5, and O6 bridge three BO_4 tetrahedra simultaneously ($O^{[3]}$), while all other oxygen ions bridge two BO_x units ($O^{[2]}$). A differentiation between the differently coordinated oxygen atoms is depicted in Figs. 2 and 3 ($O^{[2]}$: dark corners of tetrahedra and small dark spheres; $O^{[3]}$: light corners of tetrahedra). Under high-pressure, higher coordination numbers are often favoured in comparison with compounds under normal pressure [29]. HP-LiB_3O_5 is the first example in the chemistry of ternary alkali borates exhibiting threefold bridging oxygen atoms [30].

In the distorted tetrahedral BO_4 groups of HP-LiB_3O_5, the B–O distances vary from 140.9(1)–159.9(1) pm with an average value of 148.1 pm (Table 4). This is slightly larger than the known average value of 147.6 pm for BO_4 tetrahedra in borates [31,32]. Due to the distortion of the BO_4 groups in HP-LiB_3O_5, the distance range of the B–O bonds inside the tetrahedra is increased compared to the one in LiB_3O_5 [2] (146.2–149.3 pm, av. 147.6).

Table 2
Atomic coordinates and isotropic equivalent displacement parameters (U_{eq}/Å^2) for HP-LiB_3O_5 (space group: *Pnma*, No. 62). U_{eq} is defined as one third of the trace of the orthogonalized U_{ij} tensor.

Atom	Wyckoff site	*x*	*y*	*z*	U_{eq}
Li1	4*c*	0.2001(2)	1/4	0.6582(2)	0.0150(3)
Li2	4*c*	0.2735(3)	1/4	0.3744(2)	0.0172(4)
Li3	4*c*	0.4613(3)	1/4	0.0350(2)	0.0239(5)
Li4	4*c*	0.6025(3)	1/4	0.5432(2)	0.0144(3)
O1	8*d*	0.06569(5)	0.05673(6)	0.61941(3)	0.00564(8)
O2	8*d*	0.15680(6)	0.06739(6)	0.44691(3)	0.00666(8)
O3	8*d*	0.16140(6)	0.05990(6)	0.03822(3)	0.00618(8)
O4	8*d*	0.19187(5)	0.03458(6)	0.17941(3)	0.00540(8)
O5	8*d*	0.19241(5)	0.54412(6)	0.31467(3)	0.00533(8)
O6	8*d*	0.44274(5)	0.05436(6)	0.24903(2)	0.00472(8)
O7	8*d*	0.44853(5)	0.55702(6)	0.38006(3)	0.00581(8)
O8	4*c*	0.00471(7)	1/4	0.11672(4)	0.0062(2)
O9	4*c*	0.10605(8)	1/4	0.77031(4)	0.0061(2)
O10	4*c*	0.16293(7)	1/4	0.28090(4)	0.0057(2)
O11	4*c*	0.30222(8)	1/4	0.53484(4)	0.0083(2)
O12	4*c*	0.35324(7)	1/4	0.92406(4)	0.0057(2)
O13	4*c*	0.39157(8)	1/4	0.13853(4)	0.0059(2)
B1	8*d*	0.07074(8)	0.07487(8)	0.10962(4)	0.0058(2)
B2	8*d*	0.10469(8)	0.57819(8)	0.39307(4)	0.0054(2)
B3	8*d*	0.12095(8)	0.07931(8)	0.25610(4)	0.0051(2)
B4	8*d*	0.26191(8)	0.08183(9)	0.50769(4)	0.0064(2)
B5	8*d*	0.36800(7)	0.07825(8)	0.16876(4)	0.0051(2)
B6	8*d*	0.37546(8)	0.58382(8)	0.30630(4)	0.0053(2)

Table 4
Interatomic distances (pm) in HP-LiB_3O_5, derived from single crystal data of HP-LiB_3O_5.

Li1–O1 (2*x*)	196.1(2)	Li2–O10	185.6(2)	Li3–O13	187.9(2)
Li1–O9	208.8(2)	Li2–O8	192.5(2)	Li3–O12	211.5(2)
Li1–O11	229.2(2)	Li2–O2 (2*x*)	210.5(2)	Li3–O2 (2*x*)	215.7(2)
Li1–O4 (2*x*)	236.9(2)		Ø=199.8		Ø=207.7
	Ø=217.3				
Li4–O7 (2*x*)	202.1(2)				
Li4–O3 (2*x*)	207.3(2)				
Li4–O12	215.6(2)				
Li4–O11	249.6(2)				
	Ø=214.0				
B1–O3	144.9(1)	B2–O1	143.9(1)	B3–O4	148.8(1)
B1–O4	159.9(1)	B2–O2	150.8(1)	B3–O5	150.1(1)
B1–O7	143.7(1)	B2–O5	155.9(1)	B3–O6	149.3(1)
B1–O8	144.4(1)	B2–O12	145.3(1)	B3–O10	140.9(1)
	Ø=148.2		Ø=149.0		Ø=147.3
B5–O1	144.2(1)	B6–O5	155.5(1)	B4–O2	136.9(1)
B5–O4	151.0(1)	B6–O6	154.6(1)	B4–O3	135.7(1)
B5–O6	152.9(1)	B6–O7	142.5(1)	B4–O11	140.1(1)
B5–O13	141.9(1)	B6–O9	141.5(1)		Ø=137.6
	Ø=147.5		Ø=148.5		

Table 3
Anisotropic displacement parameters (U_{ij}/Å^2) for HP-LiB_3O_5 (space group: *Pnma*, no. 62).

	U_{11}	U_{22}	U_{33}	U_{23}	U_{13}	U_{12}
Li1	0.0192(9)	0.0095(7)	0.0163(9)	0	−0.0008(7)	0
Li2	0.0145(8)	0.023(2)	0.0140(8)	0	−0.0030(7)	0
Li3	0.031(2)	0.029(2)	0.0120(9)	0	0.0034(8)	0
Li4	0.0206(9)	0.0095(7)	0.0132(8)	0	−0.0011(7)	0
O1	0.0049(2)	0.0056(2)	0.0064(2)	0.0013(2)	−0.0006(2)	0.0006(2)
O2	0.0081(2)	0.0053(2)	0.0066(2)	−0.0012(2)	−0.0026(2)	0.0002(2)
O3	0.0076(2)	0.0055(2)	0.0055(2)	−0.0001(2)	0.0016(2)	0.0012(2)
O4	0.0043(2)	0.0075(2)	0.0043(2)	−0.0001(2)	0.0001(2)	−0.0002(2)
O5	0.0045(2)	0.0065(2)	0.0050(2)	−0.0016(2)	0.0004(2)	−0.0010(2)
O6	0.0042(2)	0.0055(2)	0.0044(2)	0.0009(2)	−0.0000(2)	−0.0006(2)
O7	0.0064(2)	0.0060(2)	0.0050(2)	−0.0004(2)	−0.0010(2)	0.0017(2)
O8	0.0066(2)	0.0039(2)	0.0080(3)	0	0.0009(2)	0
O9	0.0080(2)	0.0037(2)	0.0065(2)	0	−0.0007(2)	0
O10	0.0064(2)	0.0036(2)	0.0072(2)	0	−0.0011(2)	0
O11	0.0114(3)	0.0042(2)	0.0092(3)	0	−0.0038(2)	0
O12	0.0072(2)	0.0036(2)	0.0063(2)	0	0.0010(2)	0
O13	0.0075(2)	0.0040(2)	0.0060(2)	0	0.0001(2)	0
B1	0.0058(2)	0.0056(2)	0.0058(2)	−0.0003(2)	0.0004(2)	−0.0002(2)
B2	0.0057(2)	0.0048(2)	0.0056(2)	−0.0002(2)	−0.0003(2)	0.0003(2)
B3	0.0050(2)	0.0053(2)	0.0052(2)	0.0002(2)	0.0002(2)	0.0001(2)
B4	0.0070(2)	0.0054(2)	0.0066(2)	−0.0001(2)	−0.0014(2)	−0.0001(2)
B5	0.0051(2)	0.0051(2)	0.0050(2)	0.0000(2)	−0.0000(2)	0.0001(2)
B6	0.0052(2)	0.0049(2)	0.0057(2)	0.0002(2)	0.0001(2)	0.0003(2)

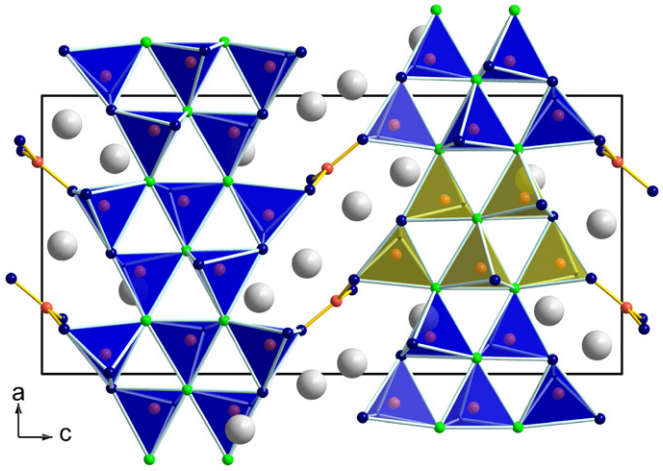

Fig. 2. Crystal structure of HP-LiB_3O_5 along [0 $\bar{1}$ 0], which exhibits layers built up from segments of corner-sharing BO_4 tetrahedra. The layers are linked through BO_3 groups. One segment of corner-sharing BO_4 tetrahedra is highlighted. Twofold coordinated oxygen ions: dark corners of tetrahedra and small dark spheres; threefold coordinated oxygen ions: light corners of tetrahedra; Li^+: large light spheres; B^{3+}: center of tetrahedra and small light spheres.

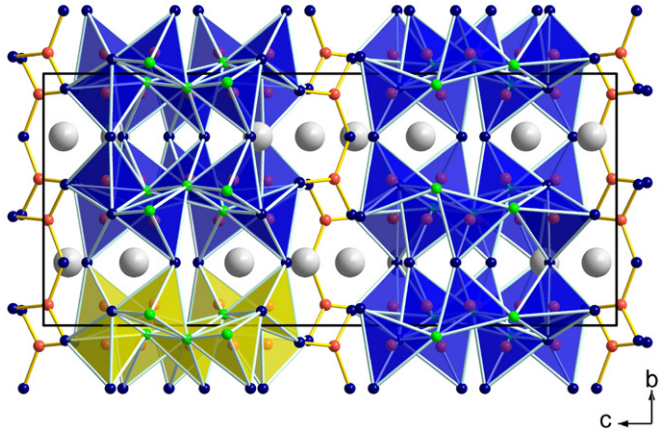

Fig. 3. Crystal structure of HP-LiB_3O_5 with a view along [$\bar{1}$ 0 0]. One ribbon of corner-sharing BO_4 tetrahedra is highlighted. Twofold coordinated oxygen ions: dark corners of tetrahedra and small dark spheres; threefold coordinated oxygen ions: light corners of tetrahedra; Li^+: large light spheres; B^{3+}: center of tetrahedra and small light spheres.

The B–O bond lengths in the BO_3 unit of HP-LiB_3O_5 vary from 135.7(1) to 140.1(1) pm with a mean value of 137.6 pm, which is also slightly increased compared to the average value in the literature (137.0 pm) [33]. The increased average bond length parallels with a slight deflection (3.8 pm) of B4 out of the plane spanned by the three oxygen atoms of the BO_3 unit. A distortion of the planarity of BO_3 units is a common feature in borates, if an additional oxygen atom is relatively close to B (B–O $\leq$ 3.0 Å) and approximately over the barycenter of the BO_3 unit [33]. In the case of HP-LiB_3O_5, this additional oxygen atom is O1 (B4–O1: 253.2(1) pm). Compared to the normal pressure compound LiB_3O_5 [2], which exhibits B–O distances of 134.6–141.0 pm for the trigonal planar BO_3 groups (av. 137.1 pm), the distance range for these units is more or less the same than the one in HP-LiB_3O_5.

One-half of the lithium ions is coordinated octahedrally by six oxygen atoms (Li1, Li4), and the other one is surrounded by four oxygen atoms in a distorted tetrahedral way (Li2, Li3) (Fig. 4). In contrast, the ambient pressure phase LiB_3O_5 [2] exhibits only fourfold coordinated lithium ions. In HP-LiB_3O_5, the Li–O distances of the sixfold coordinated metal cations range from 196.1(2) to

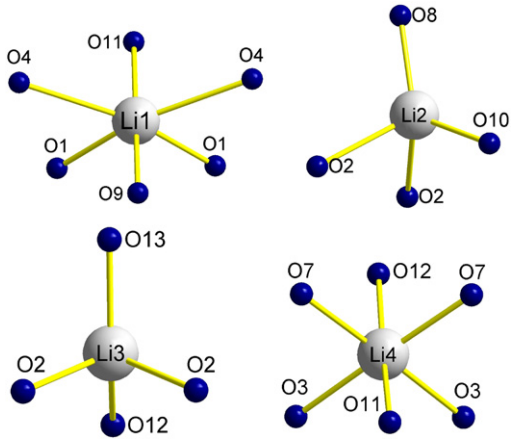

Fig. 4. Coordination spheres of the lithium ions in HP-LiB_3O_5.

249.6(2) pm with a mean value of 215.7 pm. This value is within the range of the average Li–O distances of sixfold coordinated lithium ions, e.g. $CoLiO_2$ (209.2 pm) [34], or $Li_{14}Be_5B(BO_3)_9$ (223.0 pm) [35]. For the fourfold coordinated Li^+ ions, the Li–O bond-lengths range from 185.6(2) to 215.7(2) pm with a mean value of 203.8 pm, which also stays well within the range of mean Li–O bond distances for a fourfold coordination in lithium compounds, e.g. 204.4 pm in the normal pressure phase LiB_3O_5 [2].

Additionally, we calculated bond-valence sums for HP-LiB_3O_5 with the help of the bond-length/bond-strength (ΣV) [36,37] and the CHARDI concept (*Char*ge *di*stribution in solids, ΣQ) [38]. The formal ionic charges of the atoms are consistent within the limits of the concepts (Table 5).

MAPLE values (*Ma*delung *P*art of *L*attice *E*nergy) [39–41] for HP-LiB_3O_5 were compared with those of the high-pressure modifications B_2O_3-II [42] and HP-Li_2O [43]. It is well founded by the additive potential of the MAPLE values, that allows to calculate hypothetical values for HP-LiB_3O_5 starting from the binary oxides. We obtained a value of 34,629 kJ/mol for HP-LiB_3O_5 in comparison to 34,724 kJ/mol (deviation: 0.3%), starting from the binary oxides ($1 \times$ HP-Li_2O [43] (3633 kJ/mol)$+3 \times$ B_2O_3-II [42] (21,938 kJ/mol)).

3.2. IR spectroscopy

A FTIR spectrum of a HP-LiB_3O_5 single crystal was recorded in reflectance with a Bruker Vertex 70 FTIR spectrometer (resolution $\sim$0.5 cm^{-1}), attached to a Hyperion 3000 microscope in a spectral range of 550–7000 cm^{-1}. Sixty-four scans for the sample and the background were acquired. The spectrum was deconvoluted assuming a polynomial background and folded Gaussian–Lorentzian band functions. The reflectance spectrum in the range from 1500 to 550 cm^{-1} is given in Fig. 5. The experimentally determined band positions are displayed in Table 6. The band assignments were done by quantum-mechanical calculations of harmonic vibrational frequencies at the Γ point, which were computed from first principles, using the program CRYSTAL 09 [44–46], Gaussian basis sets, and the B3LYP Hybrid HF-DFT functional. Both, IR and Raman spectra were assigned from the same calculation.

The calculations of the irreducible representation of HP-LiB_3O_5 in the point group D_{2h} yielded a very high number of 432 theoretically possible vibrational modes

$$\Gamma_{vib} = 59A_g + 49A_u + 49B_{1g} + 59B_{1u} + 49B_{2g} + 59B_{2u} + 59B_{3g} + 49B_{3u}$$

The 216 *u*-modes are IR-active and the 216 remaining *g*-modes are Raman-active. The calculations showed that the 49 A_u modes

Table 5
Charge distribution in HP-LiB_3O_5, calculated with the CHARDI concept (ΣQ) [38] and the bond-length/bond-strength concept (Σ*V*) [36,37].

	Li1	Li2	Li3	Li4	B1	B2	B3	B4	B5	B6
$\sum Q$	+0.99	+0.94	+0.93	+0.96	+2.95	+3.01	+3.14	+2.96	+2.99	+3.04
$\sum V$	+0.99	+1.10	+0.81	+1.05	+3.01	+2.93	+3.05	+2.97	+3.04	+2.98
	O1	O2	O3	O4	O5	O6	O7	O8	O9	O10
ΣQ	−2.06	−2.06	−2.12	−1.79	−1.73	−1.82	−2.06	−2.04	−2.16	−2.28
Σ*V*	−1.92	−2.03	−2.04	−2.04	−1.97	−1.99	−1.92	−1.93	−1.96	−2.15
	O11	O12	O13							
ΣQ	−1.89	−2.09	−2.29							
Σ*V*	−2.01	−1.93	−2.09							

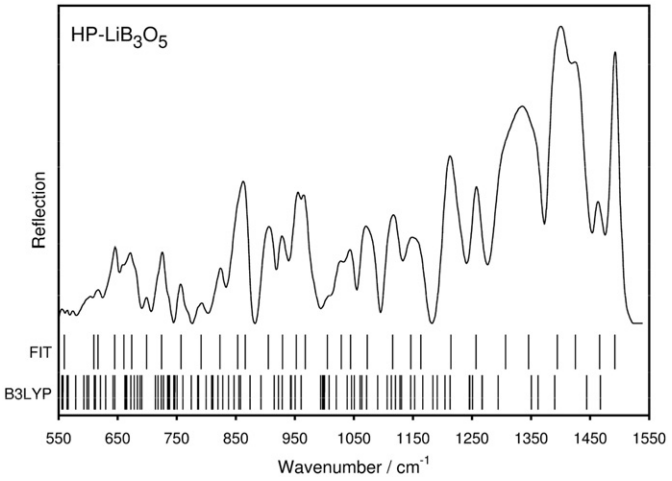

Fig. 5. FTIR reflectance spectrum of a single crystal of HP-LiB_3O_5. The vertical lines represent the wavenumber of bands derived by spectrum deconvolution (FIT) and quantum-mechanical calculations (B3LYP).

are inactive; accordingly, the experimentally determined reflectance spectrum shows a slightly lower number of bands compared to the Raman spectrum (Figs. 5 and 6). Despite of this, the large number of 167 IR-active bands prevents a complete assignment of all bands to vibrational modes. However, with some uncertainty, most observed bands were assignable (Table 6).

Usually, IR bands in the region between 800 and 1600 cm^{-1} are typical for stretching vibrations of the B–O units. Absorptions of BO_4 tetrahedra dominate at wavenumbers 800–1100 cm^{-1} [47–49], whereas BO_3 units are expected at 1200–1450 cm^{-1} [50–53]. OB_3 units ($O^{[3]}$) were postulated to absorb in the same wavenumber range as BO_3 units [30]. The assignment of the IR-bands of HP-LiB_3O_5 by comparing the measured spectrum with the calculated one, led to astonishing insights, especially for OB_3 and BO_4 units.

In the spectrum of HP-LiB_3O_5 (Fig. 5, Table 6), the bands in the high wavenumber range are related to B–O and O–B–O stretching modes of BO_3 units. Concerning the OB_3 units, calculations showed that absorptions are expected in the range of 600–1150 cm^{-1}. This leads to the conclusion that BO_3 and OB_3 groups, despite analogous geometry and similar force constants, do not absorb in the same range, at least for the structure of HP-LiB_3O_5. At 1307 cm^{-1}, the first band, which can be partially assigned to vibrations of BO_4 units, is observed. This is about 200 wavenumbers higher than normally expected for BO_4 groups, and presumably caused by the very short B3–O10 bond of the distorted tetrahedron in this high-pressure phase. Bands at lower wavenumbers result almost exclusively from motions of boron in tetrahedral coordination with the exception of two bands at 929 and 724 cm^{-1}, which are assigned to B–O–B stretching and bending modes. Starting with the band at 1147 cm^{-1}, O–B–O bending vibrations become involved. The band at 1005 cm^{-1} can be assigned to the first pure B–O–B bending vibration. Bands towards lower wavenumber become more and more dominated by bending vibrations. However, bands with B–O stretching mode participation are also observed at 823 and 660 cm^{-1}. At lower wavenumbers, bands result from B–O–B, O–B–O, and B–O–Li bending and stretching vibrations and clear assignments become increasingly difficult. The band at 724 cm^{-1} for example possibly results from B–O–B, O–Li, B–O–Li, B–O and O–B–O stretching and bending vibrations. The band at 645 cm^{-1} shows components of vibrations with both stretching and bending character (named "other" in Table 6). Bands in the area of the lower wavenumber limit have frequently Li–O stretching and O–Li–O bending vibration components.

In the range of 3000–3500 cm^{-1}, several sharp bands were detected, most probably from H_2O or OH molecules in the

Table 6
Wavenumbers and assignment of FTIR-reflection bands in the spectrum of a single crystal of HP-LiB_3O_5.

Band	Assignment
559	b(O–Li–O),s(B–Li–B),s(O–Li)
610	s(O–Li),ob(O–B–O)$_{OB3}$,sb(B–O)
617	bo(O–B–O),s(O–Li)
645	b(O–B–O)$_{OB3}$,ob(B–O–Li),b(B–O)
660	s(B–O)$_4$,s(O–Li),b(O–B–O)
674	bs(O–B–O)$_{OB3}$,o(B–O–Li)
699	o(B–O–Li)
724	s(B–O–B),s(O–Li),bs(B–O–Li),b(O–B–O)$_{OB3}$,s(B–O),b(B–O–B)$_{BO3}$
757	sb(O–B–O),s(B–O–B)$_{OB3}$,s(B–O)$_4$
792	b(O–B–O),b(B–O–B)$_{OB3}$,b(B–O–Li)
823	s(O–B–O)$_{OB3}$,s(B–O),bs(B–O–B)
853	s(B–O)$_{OB3}$,s(O–B–O)$_{OB3}$,s(B–O–B)$_{OB3}$
866	s(B–O–Li),b(O–B–O)
905	b(O–B–O),s(B–O–Li)
929	s(B–O–B)$_{BO3}$,bs(B–O–B)$_{OB3}$,s(B–O–Li)
953	s(B–O–Li),b(O–B–O)$_{OB3}$,b(B–O–B)$_{OB3}$
968	b(B–O–B)
1005	b(B–O–B)$_{OB3}$,s(B–O–Li)
1029	s(B–O)$_4$
1045	s(O–B–O)$_{OB3}$,s(B–O)$_{OB3}$
1073	s(B–O)$_{OB3}$,b(B–O–B)$_{OB3}$
1116	s(O–B–O),s(B–O)$_4$,b(O–B–O)$_{OB3}$,b(B–O–B)$_{OB3}$
1147	sb(O–B–O)$_{OB3}$,s(B–O)$_4$
1164	s(B–O–Li)
1214	s(B–O)$_4$
1257	s(O–B–O),s(B–O)$_{BO3}$,s(B–O–Li)
1307	s(O–B–O)$_{BO3}$,s(B–O)$_4$
1346	s(O–B–O)$_{BO3}$
1395	s(O–B–O)$_{BO3}$,s(B–O)$_{BO3}$
1425	s(B–O)$_{BO3}$
1466	s(B–O)$_{BO3}$
1492	s(B–O)$_{BO3}$

s—stretching; b—bending; o—other; in brackets pairs of bonded atoms with large relative motion between them; subscript 4, BO3, and OB3 refer to BO_4, BO_3, and OB_3 groups.

structure. The comparable low intensity of these bands suggests H_2O contents below 1%.

3.3. Raman spectroscopy

A confocal Raman spectrum of a single crystal of HP-LiB_3O_5 in the range of 100–4000 cm^{-1} was obtained with a Horiba Jobin Yvon LabRam-HR 800 Raman micro-spectrometer. The sample was excited by the 532 nm emission line of a 30 mW Nd–YAG-laser under an Olympus 100× objective (numerical aperture = 0.9). The size and power of the laser spot on the surface were approximately 1 μm and 5 mW, respectively. The scattered light was dispersed by a grating with 1800 lines mm^{-1} and collected by a 1024 × 256 open electrode CCD detector. The spectral resolution, determined by measuring the Rayleigh line, was about 1.4 cm^{-1}. Polynomial and convoluted Gauss–Lorentz functions were applied for background correction and band fitting. The wavenumber accuracy of about 0.5 cm^{-1} was achieved by adjusting the zero-order position of the grating and regularly checked by a Neon spectral calibration lamp.

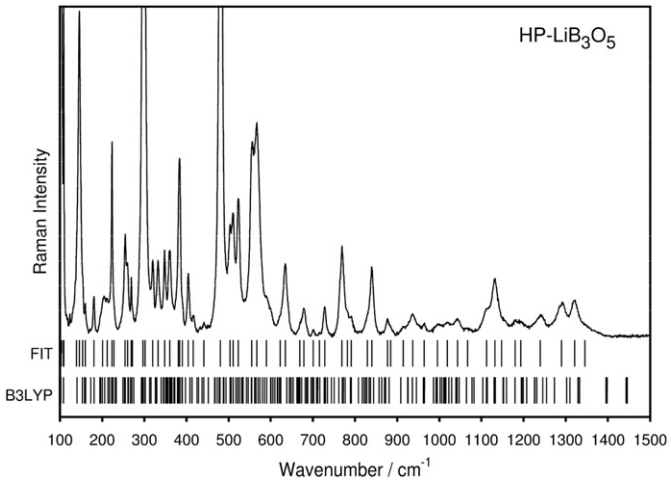

Fig. 6. Raman spectrum of a single crystal of HP-LiB_3O_5. The vertical lines represent the wavenumber of bands derived by spectrum deconvolution (FIT) and quantum-mechanical calculations (B3LYP). For better visibility, the intensity axis is cut at ~25.000 counts.

Fig. 6 shows the Raman spectrum of HP-LiB_3O_5 in the range of 100–1500 cm^{-1}, the experimentally determined band positions are displayed in Table 7. In agreement with the irreducible representation, a large number of bands were detected, complicating their assignment to calculated vibrational modes. Above 1400 cm^{-1} four modes were calculated, which do not appear in the experimental spectrum. Similar to the FTIR spectrum, bands in the high wavenumber range are related to stretching vibrations of BO_3 units. At 1240 cm^{-1}, the first band, that can be assigned to movements of BO_4 and OB_3 units, is observed. The weak bands between 600 and 1350 cm^{-1} are dominantly B–O stretching vibrations but with variable contributions of O–B–O stretching, bending, and B–O–Li vibration. Compared to the FTIR spectrum a larger number of modes between 728 and 360 cm^{-1} involves boron in threefold coordination. B–O stretching components contribute to bands at low wavenumbers, for example the band at 555 cm^{-1}. The intense band at 481 cm^{-1} is assigned to the complex bending of O–Li–O and O–B–O bonds and the stretching and bending of O–Li and Li–O–B bonds. Below 480 cm^{-1}, O–Li–O

Table 7
Wavenumbers and assignment of Raman bands in the spectrum of HP-LiB_3O_5.

Band	Assignment	Band	Assignment
103	b(O–Li–O)	567	$b(B–O–B)_{OB3}$,s(O–Li)
108	b(Li–O–B)	590	s(O–Li),$o(O–B–O)_{OB3}$,$o(B–O–Li)_{BO3}$
109	b(Li–O–B)	623	$b(B–O–B)_{OB3}$,$o(B–O–Li)_{BO3}$,$o(O–B–O)_{OB3}$
139	s(O–Li)	635	$o(O–B–O)_{BO3}$,$o(B–O–Li)_{BO3}$
146	s(O–Li)	669	bs(O–B–O),s(B–O), $b(B–O–Li)_{BO3}$,s(O–Li)
154	b(Li–O–B)	679	$bs(O–B–O)_{OB3}$
160	s(O–Li–O),b(Li–O–B)	701	$s(B–O–B)_{BO3}$,$b(B–O–Li)_{BO3}$
180	b(O–Li–O)	715	b(O–B–O)
201	bs(O–Li–O),b(Li–O–B)	728	$s(B–O)_4$,s(O–Li–O),s(O–Li),$b(B–O–B)_{BO3}$
212	b(O–Li–O),b(Li–O–B)	769	$sb(O–B–O)_{OB3}$,$sb(B–O–B)_{OB3}$,b(B–O–Li)
223	bs(O–Li–O),b(Li–O–B)	782	s(B–O–Li)
228	bs(O–Li–O),s(O–Li),b(Li–B–O),b(Li–O–Li)	791	$sb(B–O–B)_{OB3}$,$s(O–B–O)_{OB3}$,$s(B–O)_{OB3}$
254	bs(O–Li–O),b(B–Li–B),b(Li–O–B)	829	$b(B–O–Li)$,$s(B–O)_4$,b(B–O–B),o(O–B–O)
260	bs(O–Li–O),b(Li–O–B)	840	$s(B–O)_{OB3}$,bs(O–B–O),b(B–O–B)
269	b(O–Li–O),s(Li–O–Li)	877	$s(B–O)_{OB3}$,s(B–O–Li),$bs(O–B–O)_{OB3}$,b(B–O–B)
272	b(O–Li–O),s(Li–O–Li)	884	$s(B–O–B)_{OB3}$
297	b(O–Li–O),s(O–Li),b(Li–O–B),bs(Li–O–Li)	914	$s(B–O)_{OB3}$,s(O–B–O)
302	b(O–Li–O),b(B–Li–O)	937	$s(B–O)_4$,s (O–B–O)
320	s(Li–Li),b(O–Li–O)	964	$s(B–O)_4$,$s(O–B–O)_{OB3}$,b(B–O–B)
333	b(O–Li–B),sb(O–Li–O)	996	s(B–O–Li)
348	$ob(O–Li–O)$,$o(O–B–O)_{OB3}$,s(O–Li)	1019	s(B–O),$s(O–B–O)_{OB3}$,$b(B–O–B)_{OB3}$
360	b(Li–O–B),s(O–Li–O),b(Li–O–Li)	1043	$sbo(O–B–O)_{OB3}$
381	bs(O–Li–O)	1067	s(O–B–O)
384	bs(O–Li–O)	1112	$s(B–O)_4$,$bos(O–B–O)_{OB3}$
390	b(O–Li–O)	1132	b(B–O–B),$b(O–B–O)_{OB3}$,$s(B–O)_{OB3}$,s(O–B–O)
404	s(O–Li–O)	1148	$s(O–B–O)$,$s(B–O)_4$,s(B–O–B)
416	b(Li–O–Li)	1180	$s(B–O)_4$
441	sb(O–Li–O),s(O–Li)	1194	$s(B–O–Li)$,$s(B–O)_4$,$b(O–B–O)_{OB3}$
481	$b(O–Li–O)$,$b(O–B–O)_{OB3}$,s(O–Li),sb(Li–O–B)	1240	$s(B–O)_4$
503	b(O–Li–O)	1290	s(B–O)
511	s(O–Li–O)	1321	$s(B–O)_{BO3}$,$s(O–B–O)_{BO3}$
523	s(O–Li),s(Li–O–B),b(O–Li–O)	1346	$s(B–O)_{BO3}$,$s(O–B–O)_{BO3}$
555	$so(O–B–O)_{OB3}$,$s(O–B–O)_{OB3}$,$s(B–O)_4$		

s—stretching; b—bending; o—other; in brackets pairs of bonded atoms with large relative motion between them; subscript 4, BO3, and OB3 refer to BO4, BO3, and OB3 groups.

and Li–O–Li bending and stretching modes instead of the O–B–O modes dominate, like the intense band around 300 cm^{-1} and the most intense band in the spectrum at 103 cm^{-1}. Some bands in this low wavenumber range are pure O–Li stretching modes (139+146 cm^{-1}), very rarely Li–Li (320 cm^{-1}) stretching and B–Li–B bending modes occur.

In analogy to the FTIR-spectrum, several bands between 3000 and 3500 cm^{-1} were observed, which are interpreted as low amounts of H_2O or OH molecules in the crystal structure. These molecules can be released during heating, which was confirmed by heating up a crystal aggregate to 450 °C and Raman measurements after cooling down to room temperature, clearly showing a decreased intensity of these bands.

3.4. Thermal behavior

Considering the high-pressure/high-temperature conditions during the synthesis, the assumed metastable character of HP-LiB_3O_5 was investigated. The temperature stability of the borate HP-LiB_3O_5 was examined via an *in-situ* temperature-programmed X-ray powder diffraction experiment in air, which was carried out on a Stoe Stadi P powder diffractometer (Mo$K\alpha_1$; λ=70.93 pm) with a computer controlled Stoe furnace. The sample was enclosed in a silica glass capillary and heated from room temperature to 500 °C in steps of 100 °C and from 500 to 1100 °C in steps of 50 °C. After reaching 1100 °C, the sample was cooled down to 500 °C in steps of 50 °C and further on to room temperature in steps of 100 °C. At each step, a powder diffraction pattern was recorded. Fig. 7 shows the temperature dependent powder patterns of the investigated sample. The high-temperature powder patterns reveal a temperature stability of the borate HP-LiB_3O_5 up to a temperature of 550 °C. The rising of temperature up to 900 °C led to five different powder patterns, which are due to phase transitions into various lithium borates. In the temperature range of 700–800 °C the powder patterns revealed the formation of the normal pressure phase LiB_3O_5. Higher temperatures and subsequent cooling led to an amorphous product. Remaining reflections come from the furnace.

As the Li^+ ions are situated in relatively large channels, ionic conductivity would be thinkable. For a first examination of the ion mobility of Li^+ within the channels along the *b*-axis in HP-LiB_3O_5, high-temperature single crystal experiments were performed. The data were recorded at elevated temperatures on a Stoe IPDS-II single crystal diffractometer (Mo$K\alpha$, λ=0.71073 Å, graphite monochromator), modified according to Krüger and Breil [54]. For this purpose, the crystal was clamped in the constricting part of a 0.1 mm silica-glass capillary. A heatstream device (as provided by Stoe) was used for the high-temperature single-crystal diffraction experiment. This furnace (mounted underneath the sample on the omega axis) supplied a vertical flow of hot nitrogen gas to heat the sample. Data were collected at temperatures of 25, 150, 300 as well as 450 °C. Fig. 8 compares the 90% probability ellipsoids of HP-LiB_3O_5 at room temperature and at 450 °C. No obvious mobility of Li^+ along the channels could be detected.

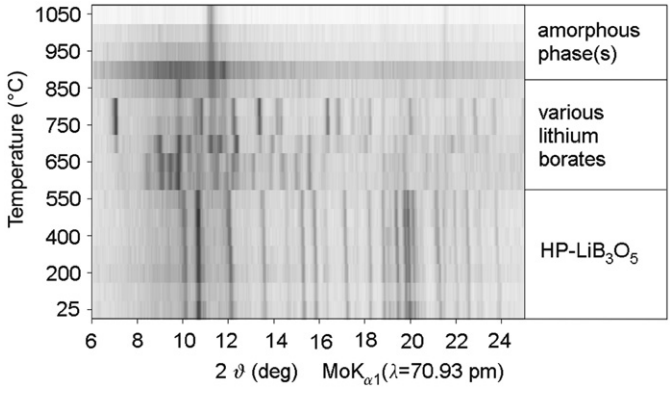

Fig. 7. Temperature-programmed diffraction patterns of HP-LiB_3O_5.

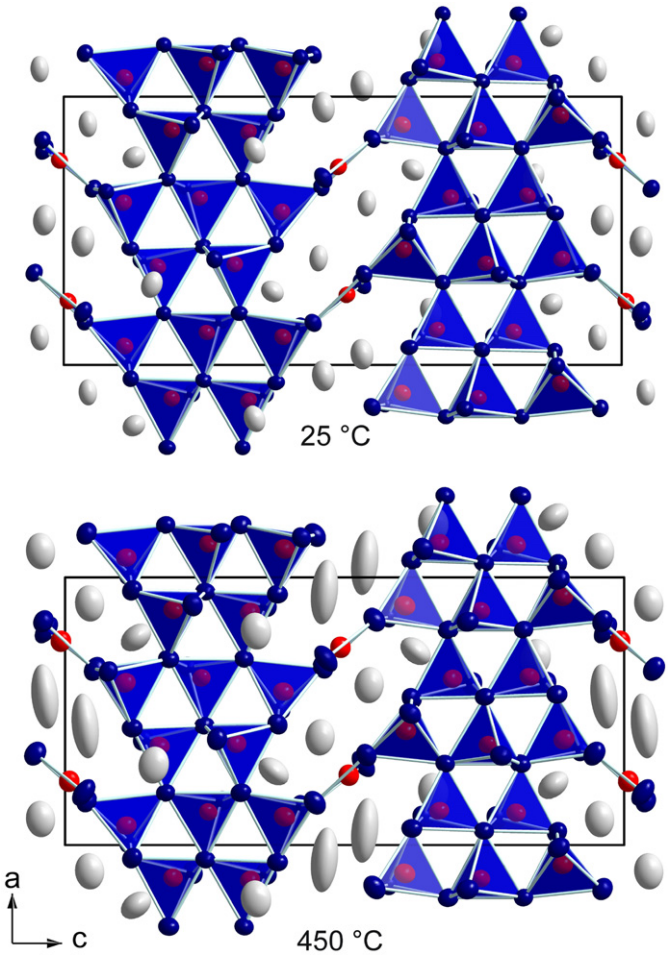

Fig. 8. Comparison of the 90% probability ellipsoids of HP-LiB_3O_5 at room temperature (top) and at 450 °C (bottom).

4. Conclusions

The new lithium borate HP-LiB_3O_5 is built up from layers of corner-sharing BO_4 tetrahedra, which are interconnected via trigonal-planar BO_3 units, generating channels along the *b*-axis, in which the Li^+ ions are situated. As not uncommon for high-pressure phases, the crystal structure comprises threefold coordinated oxygen atoms ($O^{[3]}$). For the future, both an increase and a reduction of the boron content is planned in order to explore the phase diagram of the system Li_2O–B_2O_3 in more detail. Especially in the boron-oxide-rich part of the system, the parameter pressure may be crucial for the synthesis of new crystalline compounds, repressing the perpetual tendency of glass formation in borates.

Acknowledgments

Special thanks go to Dr. G. Heymann for collecting the single crystal data. Furthermore, we would like to thank S. Sedlmaier (University of Munich (LMU)) for performing the temperature-programmed X-ray powder diffraction experiments and E. Arroyabe

performing the temperature-programmed X-ray single-crystal diffraction experiments. This work was financially supported by the Austrian Ministry of Science (BMWF) as part of the Uniinfrastrukturprogramm of the Forschungsplattform Scientific Computing at LFU Innsbruck.

Appendix A. Supplementary material

Supplementary data associated with this article can be found in the online version at doi:10.1016/j.jssc.2011.07.011.

References

[1] P. Becker, Adv. Mater. 10 (1998) 979–992.
[2] H. König, R. Hoppe, Z. Anorg. Allg. Chem. 439 (1978) 71–79.
[3] C.T. Chen, Y.C. Wu, A.D. Jiang, B.C. Wu, G.M. You, R.K. Li, S.J. Lin, J. Opt. Soc. Am. 6B (1989) 616–621.
[4] K. Kato, IEEE J. Quantum Electron. 26 (1990) 1173–1175.
[5] T. Ukachi, R.J. Lane, W.R. Bosenberg, C.L. Tang, Appl. Phys. Lett. 57 (1990) 980–982.
[6] S. Matyjasik, Yu.V. Shaldin, Phys. Solid State 43 (2001) 1464–1467.
[7] Y. Wang, Y.J. Jiang, Y.L. Liu, F.Y. Cai, L.Z. Zeng, Appl. Phys. Lett. 67 (1995) 2462–2464.
[8] I.N. Ogorodnikov, L.I. Isaenko, A.V. Kruzhalov, A.V. Porotnikov, Radiat. Meas. 33 (2001) 577–581.
[9] I.N. Ogorodnikov, V.Yu. Yakovlev, L.I. Isaenko, Phys. Solid State 45 (2003) 845–853.
[10] J. Krogh-Moe, Acta Crystallogr. 15 (1962) 190–193.
[11] J. Krogh-Moe, Acta Crystallogr. Sect. 24B (1968) 179–181.
[12] N. Sennova, R. Bubnova, J. Shepelev, S. Filatov, O. Yakovleva, J. Alloys Compd. 428 (2007) 290–296.
[13] N. Sennova, R.S. Bubnova, G. Cordier, B. Albert, S.K. Filatov, L. Isaenko, Z. Anorg. Allg. Chem. 634 (2008) 2601–2607.
[14] W.H. Zachariasen, Acta Crystallogr. 17 (1964) 749–751.
[15] A. Kirfel, G. Will, R.F. Stewart, Acta Crystallogr. Sect. 39B (1983) 175–185.
[16] A. Jiang, S. Lei, Q. Huang, T. Chen, D. Ke, Acta Crystallogr. Sect. 46C (1990) 1999–2001.
[17] N. Kawai, S. Endo, Rev. Sci. Instrum. 41 (1970) 1178–1181.
[18] D.C. Rubie, Phase Transitions 68 (1999) 431–451.
[19] H. Huppertz, Z. Kristallogr. 219 (2004) 330–338.
[20] D. Walker, M.A. Carpenter, C.M. Hitch, Am. Mineral. 75 (1990) 1020–1028.
[21] D. Walker, Am. Mineral. 76 (1991) 1092–1100.
[22] P.-E. Werner, L. Eriksson, M. Westdahl, J. Appl. Crystallogr. 18 (1985) 367–370.
[23] Stoe WinXpow, v1.2, Stoe+Cie GmbH, Darmstadt, Germany, 2001.
[24] Z. Otwinowski, W. Minor, Methods Enzymol. 276 (1997) 307–326.
[25] A.L. Spek, Platon—A Multipurpose Crystallographic Tool, Utrecht University, Netherlands, 2002.
[26] G.M. Sheldrick, SHELXS-97 and SHELXL-97, Program suite for the solution and refinement of crystal structures, University of Göttingen, Göttingen, Germany, 1997.
[27] G.M. Sheldrick, Acta Crystallogr. Sect. 64A (2008) 112–122.
[28] P.T. Moseley, in: J.L. Sudworth, A.R. Tilley (Eds.), The Sodium Sulfur Battery, Chapman and Hall, London, New York, 1985, p. 19.
[29] H. Huppertz, Chem. Commun. 47 (2011) 131–140.
[30] H. Huppertz, Z. Naturforsch. 58B (2003) 257–265.
[31] E. Zobetz, Z. Kristallogr. 191 (1990) 45–57.
[32] F.C. Hawthorne, P.C. Burns, J.D. Grice, in: 2nd ed.,in: E.S. Grew, L.M. Anovitz (Eds.), The Crystal Chemistry of Boron, in Boron: Mineralogy, Petrology and Geochemistry, vol. 33, Mineralogical Society of America, Washington, 1996, p. 41.
[33] E. Zobetz, Z. Kristallogr. 160 (1982) 81–92.
[34] H.J. Orman, P.J. Wiseman, Acta Crystallogr. Sect. 40C (1984) 12–14.
[35] J.L. Luce, K.I. Schaffers, D.A. Keszler, Inorg. Chem. 33 (1994) 2453–2455.
[36] I.D. Brown, D. Altermatt, Acta Crystallogr. Sect. 41B (1985) 244–247.
[37] N.E. Brese, M. O'Keeffe, Acta Crystallogr. Sect. 47B (1991) 192–197.
[38] R. Hoppe, S. Voigt, H. Glaum, J. Kissel, H.P. Müller, K.J. Bernet, J. Less-Common Met. 156 (1989) 105–122.
[39] R. Hoppe, Angew. Chem. 78 (1966) 52–63;
Angew. Chem. Int. Ed. 5 (1966) 95–106.
[40] R. Hoppe, Angew. Chem. 82 (1970) 7–16;
Angew. Chem. Int. Ed. 9 (1970) 25–34.
[41] R. Hübenthal, Maple—Program for the Calculation of Maple-Values, Vers. 4, University of Giessen, Germany, 1993.
[42] C.T. Prewitt, R.D. Shannon, Acta Crystallogr. Sect. 24B (1968) 869–874.
[43] A. Grzechnik, P. Bouvier, L. Farina, J. Solid State Chem. 173 (2003) 13–19.
[44] R. Dovesi, V.R. Saunders, C. Roetti, R. Orlando, C.M. Zicovich-Wilson, F. Pascale, B. Civalleri, K. Doll, N.M. Harrison, I.J. Bush, Ph. D'Arco, M. Llunell, CRYSTAL09—User's Manual, University of Torino, Torino, 2009.
[45] R. Dovesi, R. Orlando, B. Civalleri, R. Roetti, V.R. Saunders, C.M. Zicovich-Wilson, Z. Kristallogr. 220 (2005) 571–573.
[46] F. Pascale, C.M. Zicovich-Wilson, F. Lopez, B. Civalleri, R. Orlando, R. Dovesi, J. Compd. Chem. 25 (2004) 888–897.
[47] M. Ren, J.H. Lin, Y. Dong, L.Q. Yang, M.Z. Su, L.P. You, Chem. Mater. 11 (1999) 1576–1580.
[48] J.P. Laperches, P. Tarte, Spectrochim. Acta 22 (1966) 1201–1210.
[49] G. Blasse, G.P.M. van den Heuvel, Phys. Status Solidi 19 (1973) 111–117.
[50] S.D. Ross, Spectrochim. Acta 28A (1972) 1555–1561.
[51] W.C. Steele, J.C. Decius, J. Chem. Phys. 25 (1956) 1184–1188.
[52] R. Böhlhoff, H.U. Bambauer, W. Hoffmann, Z. Kristallogr. 133 (1971) 386–395.
[53] K. Machida, H. Hata, K. Okuno, G. Adachi, J. Shiokawa, J. Inorg. Nucl. Chem. 41 (1979) 1425–1430.
[54] H. Krüger, L. Breil, J. Appl. Crystallogr. 42 (2009) 140–142.